Isomerization and Fluxional Behavior of the *tetrahedro*-Triosmium–Platinum Clusters $Os_3Pt(\mu\text{-}H)_2(CO)_9(Pt\text{-}PCy_3)(Os\text{-}PR_3)$: X-ray Crystal Structure of $Os_3Pt(\mu\text{-}H)_2(CO)_9(Pt\text{-}PCy_3)(Os\text{-}PPh_3)$

Louis J. Farrugia* and Shirley E. Rae

Department of Chemistry, The University, Glasgow G12 8QQ, Scotland, U.K.

Received May 9, 1991

The 58-electron clusters $Os_3Pt(\mu\text{-}H)_2(CO)_9(Pt\text{-}PCy_3)(Os\text{-}PR_3)$ (**3a**; $R_3 = Me_2Ph$; **3b**, $R_3 = Me_3$; **3c**, $R_3 = Ph_3$; **3d**; $R_3 = {}^iPr_3$; **3e**; $R_3 = Cy_2{}^iPr$) have been synthesized by reaction of $Os_3(\mu\text{-}H)_2(CO)_9(PR_3)$ with $Pt(C_2H_4)_2(PCy_3)$, and their fluxional behavior has been examined. The structures adopted depend on the steric bulk of the phosphine PR_3. One isomer (isomer A) predominates for clusters **3a–c**, with some evidence for a very minor component. Crystal data for **3c**: monoclinic, space group $P2_1/c$, a = 12.448 (2) Å, b = 16.319 (3) Å, c = 24.936 (5) Å, β = 89.44 (1)°, V = 5065 (2) Å^3, Z = 4, and final R (R_w) values 0.031 (0.042) for 5359 independent observed data, $I \geq 3\sigma(I)$. The structure of **3c** shows that isomer A is related to the parent species $Os_3Pt(\mu\text{-}H)_2(CO)_{10}(Pt\text{-}PCy_3)$ (**1**), with a PPh_3 group substituting in a radial site. **3a–c** exhibit hydride migration, with $\Delta G^{\ddagger}$ at coalescence being 57.1, 56.5, and 55 kJ mol^{-1}, respectively. A ^{13}C EXSY spectrum of **3a** shows several independent CO exchange pathways, including a concerted migration of a hydride and rotation of the $Pt(H)(CO)(PCy_3)$ group resulting in cluster enantiomerization. Clusters **3d,e** exist as a ~1:1 mixture of two isomers in solution, isomer A and a second isomer B possessing two inequivalent $Os(\mu\text{-}H)Os$ hydrides. Isomers A and B are in rapid exchange on the NMR time scale at ambient temperatures, and a value for $\Delta G^{\ddagger}_{233}$ of 54.9 kJ mol^{-1} has been estimated for their interconversion in cluster **3d**, from analysis of the ^{31}P EXSY spectrum.

Introduction

We have previously reported dynamic ^1H and ^{13}C NMR studies on $Os_3Pt(\mu\text{-}H)_2(CO)_{10}(Pt\text{-}PCy_3)$ (**1**)[1] and the isonitrile derivative $Os_3Pt(\mu\text{-}H)_2(CO)_9(Pt\text{-}PCy_3)(Pt\text{-}CNCy)$ (**2**).[2] The inequivalent $Os(\mu\text{-}H)Pt$ and $Os(\mu\text{-}H)Os$ hydrides undergo site exchange, and the presence of the isonitrile ligand in **2** considerably raises the barrier to this migration. These systems are of interest in view of the possibility of PtL_2 rotation about the Os_3 triangle, which was first suggested by Hoffmann and Schilling in an EHMO study.[3] The variable-temperature ^{13}C NMR spectra of **1** are compatible with such a rotation,[1b] and we have recently reported[2] unambiguous evidence for the rotation of the $Pt(H)(CNCy)(PCy_3)$ unit in **2**, from the dynamic behavior of ^{187}Os–^1H couplings. With a view to investigating the effect of phosphine substitution on the fluxional behavior of these systems, we have undertaken dynamic 1D and 2D NMR studies on several phosphine derivatives of cluster **1**. In addition to the studies reported herein, we have also prepared several related (1-naphthyl)phosphine derivatives, which show a remarkable reversible cyclometalation. These will be the subject of a forthcoming publication.[4] The studies reported herein were initiated by our desire for an acceptable synthetic route to the 60-electron butterfly species $Os_3Pt(\mu\text{-}H)_2(CO)_{10}(Pt\text{-}PCy_3)(Os\text{-}PR_3)$ containing prochiral phosphines PR_3, in view of the interesting enantiomerization process proposed for the $(PCy_3)_2$ cluster.[1b]

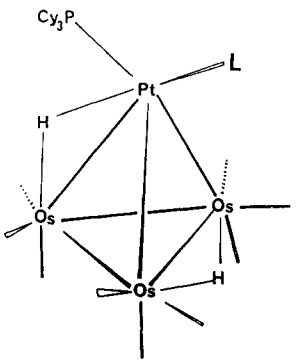

1; L = CO **2**; L = CNCy

Table I. ^1H NMR Data (Hydride Region) for $Os_3Pt(\mu\text{-}H)_2(CO)_9(Pt\text{-}PCy_3)(Os\text{-}L)$

L		δ(H1)	δ(H2)	J(Pt–H),[a] Hz	J(P–H),[a] Hz
CO[b]	**1**	-8.47	-6.84	590, 6.5	12.4
PMe_2Ph[c]	**3a**	-8.53	-6.56	578	13.4, 7.1
PMe_3[d]	**3b**	-8.59	-6.93	574	12.6, 7.3
PPh_3[e]	**3c**	-8.51	-6.33	575	11.8, 6.3
P^iPr_3[f]	**3d**				
isomer A		-8.73	-7.02	559	11.2, 7.6
isomer B[g]			-12.50		7.0
$PCy_2{}^iPr$[h]	**3e**				
isomer A		-8.69	-7.01	562	11.3, 7.0
isomer B[g]			-12.39		7.1

[a] J(Pt–H), J(P–H) given consecutively for $Pt(\mu\text{-}H)Os$ (H1) and $Os(\mu\text{-}H)Os$ (H2) resonances. [b] Reference 1b, CD_2Cl_2, 233 K. [c] $CDCl_3$, 213 K. [d] CD_2Cl_2, 235 K. [e] CD_2Cl_2, 223 K. [f] CD_2Cl_2, 213 K. [g] For isomer B the coalesced resonance for the two inequivalent $Os(\mu\text{-}H)Os$ hydrides is given (see text). [h] CD_2Cl_2, 248 K.

Results and Discussion

A series of the unsaturated 58-electron nonacarbonyl derivatives $Os_3Pt(\mu\text{-}H)_2(CO)_9(Pt\text{-}PCy_3)(Os\text{-}PR_3)$ (**3**) were prepared in high yield by the reaction of $Os_3(\mu\text{-}H)_2(CO)_9(PR_3)$[5,6] with $Pt(PCy_3)(C_2H_4)_2$. They are dark green

(1) (a) Farrugia, L. J.; Howard, J. A. K.; Mitrprachachon, P.; Stone, F. G. A.; Woodward, P. *J. Chem. Soc., Dalton Trans.* **1981**, 155. (b) Ewing, P.; Farrugia, L. J.; Rycroft, D. S. *Organometallics* **1988**, *7*, 859.
(2) Farrugia, L. J. *Organometallics* **1989**, *8*, 2410.
(3) Schilling, B. E. R.; Hoffmann, R. *J. Am. Chem. Soc.* **1979**, *101*, 3456.
(4) Rae, S. E.; Farrugia, L. J. To be published.
(5) Farrugia, L. J. *J. Organomet. Chem.* **1990**, *394*, 515.
(6) (a) Deeming, A. J.; Hasso, S. *J. Organomet. Chem.* **1976**, *114*, 313. (b) Benfield, R. E.; Johnson, B. F. G.; Lewis, J.; Raithby, P. R.; Zuccaro, C.; Hendrick, K. *Acta Crystallogr., Sect. B* **1979**, *B35*, 2210. (c) Adams, R. D.; Segmüller, B. E. *Cryst. Struct. Commun.* **1982**, *11*, 1971.

0276-7333/91/2310-3919$02.50/0

Table II. ^{31}P NMR Data for $Os_3Pt(\mu\text{-}H)_2(CO)_9(Pt\text{-}PCy_3)(Os\text{-}L)$

L		$\delta(PCy_3)$	$\delta(Os\text{-}PR_3)$	J(Pt–P)	J(P–P)
CO[a]	1	74.8		2503	
PMe_2Ph[b]	3a	70.0	-8.5	2608 (2575[c])	13
PMe_3[d]	3b	70.5	-15.1	2575 (2601[e])	11
PPh_3[f]	3c	69.6	27.4	2560 (2640[g])	14
P^iPr_3[h]	3d				
isomer A		66.9	58.5	2621, 84	13
isomer B		61.5	46.1	3269, 97	22
$PCy_2{}^iPr$[i]	3e				
isomer A		67.1	55.2	2622	14
isomer B		62.3	44.1	3253	22

[a] Reference 1a, $CDCl_3$, 298 K. [b] $CDCl_3$, 298 K. [c] 253 K. [d] CD_2Cl_2, 238 K. [e] 298 K. [f] CD_2Cl_2, 252 K. [g] 298 K. [h] CD_2Cl_2, 233 K. [i] CD_2Cl_2, 248 K.

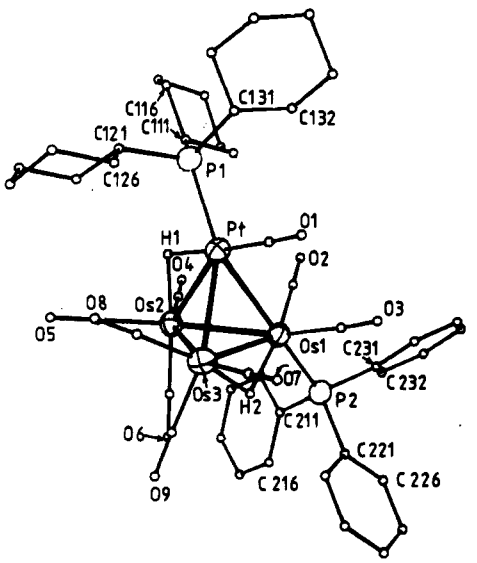

Figure 1. Molecular structure and atomic labeling scheme for $Os_3Pt(\mu\text{-}H)_2(CO)_9(Pt\text{-}PCy_3)(Os\text{-}PPh_3)$ (**3c**). Carbonyl carbon atoms have the same label as attached oxygens.

or greenish brown in color, consistent with chemical unsaturation. The structures adopted depend on the steric bulk of the phosphine PR_3. For the PMe_2Ph, PMe_3, and PPh_3 derivatives, **3a–c**, there is one predominant isomer in solution. The ^1H (hydride region) and ^{31}P NMR parameters (Tables I and II) of **3a–c** are similar to those of **1** and suggest an identical structure, with a phosphine replacing one CO ligand. In view of the ambiguity in the NMR data regarding the site of phosphine substitution (see below), an X-ray structure was carried out on **3c**, the only derivative giving suitable crystals. Further discussion of NMR data is deferred until the X-ray structure of **3c** is presented.

Molecular Structure of 3c. The molecular structure and atomic labeling scheme for **3c** is shown in Figure 1, and atomic coordinates and important metrical parameters are given in Tables III and IV, respectively. The structural analysis confirms that cluster **3c** is related to **1**[1a] and **2**.[7] The Os-bound phosphine ligand occupies a radial site[8] [trans to the Pt–Os(1) bond, Pt–Os(1)–P(2) = 170.3 (1)°] on one of the Os atoms involved in the Os(μ-H)Os bridge. The Pt–Os separations are in the normal range,[9] although,

Table III. Final Positional Parameters (Fractional Coordinates) with Esd's in Parentheses and Isotropic Thermal Parameters (Å²; Equivalent Isotropic Parameters U_{eq} for Anisotropic Atoms) for $Os_3Pt(\mu\text{-}H)_2(CO)_9(Pt\text{-}PCy_3)(Os\text{-}PPh_3)\cdot 0.5\ CH_2Cl_2$ (3c)

atom	x/a	y/b	z/c	U_{eq}[a]
Pt	0.40976 (4)	0.16725 (3)	0.32036 (2)	0.035
Os(1)	0.24296 (4)	0.26054 (3)	0.37155 (2)	0.037
Os(2)	0.41523 (4)	0.20343 (3)	0.43070 (2)	0.036
Os(3)	0.26386 (4)	0.09489 (3)	0.39262 (2)	0.042
P(1)	0.5738 (3)	0.1696 92)	0.2725 (1)	0.036
P(2)	0.1311 (3)	0.3513 (2)	0.4165 (1)	0.037
O(1)	0.2692 (8)	0.1194 (7)	0.2289 (4)	0.083
O(2)	0.3717 (8)	0.4114 (6)	0.3421 (4)	0.079
O(3)	0.0938 (11)	0.2464 (8)	0.2774 (5)	0.128
O(4)	0.5336 (8)	0.3624 (6)	0.4451 (4)	0.066
O(5)	0.5774 (10)	0.0908 (7)	0.4832 (4)	0.092
O(6)	0.2761 (8)	0.2102 (6)	0.5304 (3)	0.066
O(7)	0.0919 (10)	0.0217 (7)	0.3201 (5)	0.107
O(8)	0.4235 (10)	-0.0446 (6)	0.3900 (5)	0.098
O(9)	0.1693 (12)	0.0282 (7)	0.4955 (5)	0.112
C(1)	0.3210 (10)	0.1373 (8)	0.2642 (5)	0.054
C(2)	0.3240 (10)	0.3529 (8)	0.3512 (5)	0.052
C(3)	0.1472 (13)	0.2559 (10)	0.3141 (6)	0.077
C(4)	0.4872 (10)	0.3017 (8)	0.4393 (5)	0.045
C(5)	0.5157 (12)	0.1331 (8)	0.4631 (5)	0.061
C(6)	0.3286 (10)	0.2080 (7)	0.4922 (4)	0.044
C(7)	0.1552 (12)	0.0491 (8)	0.3480 (6)	0.063
C(8)	0.3634 (13)	0.0086 (9)	0.3904 (7)	0.073
C(9)	0.2069 913)	0.0527 (8)	0.4568 (7)	0.072
C(100)	0.990 (3)	0.349 (2)	0.097 (1)	0.09 (1)
C(111)	0.6551 (9)	0.2591 (7)	0.2896 (5)	0.042
C(112)	0.5963 (11)	0.3397 (7)	0.2878 (6)	0.056
C(113)	0.6634 (12)	0.4067 (8)	0.3145 (6)	0.063
C(114)	0.7686 (14)	0.4160 (9)	0.2879 (7)	0.079
C(115)	0.8299 (12)	0.3362 (9)	0.2873 (7)	0.075
C(116)	0.7655 (11)	0.2673 (9)	0.2636 (6)	0.063
C(121)	0.6576 (10)	0.0809 (7)	0.2889 (4)	0.041
C(122)	0.6010 (11)	0.0022 (7)	0.2753 (6)	0.062
C(123)	0.6747 (13)	-0.0712 (8)	0.2865 (7)	0.077
C(124)	0.7082 (15)	-0.0707 (11)	0.3451 (8)	0.100
C(125)	0.7670 (13)	0.0112 (11)	0.3576 (6)	0.083
C(126)	0.6957 (12)	0.0812 (8)	0.3464 (5)	0.065
C(131)	0.5527 (10)	0.1634 (7)	0.1995 (5)	0.047
C(132)	0.4992 (12)	0.2425 (8)	0.1777 (5)	0.062
C(133)	0.4668 (15)	0.2319 (11)	0.1194 (7)	0.093
C(134)	0.5620 (17)	0.2021 (12)	0.0837 (6)	0.103
C(135)	0.6093 (14)	0.1276 (11)	0.1060 (5)	0.086
C(136)	0.6467 (12)	0.1369 (8)	0.1644 (6)	0.063
C(211)	0.1858 (12)	0.3851 (9)	0.4808 (3)	0.036
C(212)	0.2861 (10)	0.4231 (6)	0.4811 (3)	0.051
C(213)	0.3306 (7)	0.4487 (6)	0.5294 (3)	0.064
C(214)	0.2746 (11)	0.4362 (8)	0.5775 (3)	0.070
C(215)	0.1743 (8)	0.3981 (4)	0.5772 (3)	0.071
C(216)	0.1299 (9)	0.3726 (8)	0.5288 (3)	0.050
C(221)	-0.0047 (5)	0.3160 (7)	0.4331 (4)	0.040
C(222)	-0.0283 (9)	0.2325 (6)	0.4359 (7)	0.068
C(223)	-0.1316 (9)	0.2067 (4)	0.4500 (5)	0.086
C(224)	-0.2114 (5)	0.2643 (6)	0.4612 (4)	0.064
C(225)	-0.1879 (9)	0.3478 (5)	0.4584 (6)	0.070
C(226)	-0.0846 (9)	0.3736 (5)	0.4444 (5)	0.054
C(231)	0.1056 (7)	0.4474 (7)	0.3813 (6)	0.039
C(232)	0.1135 (10)	0.5232 (10)	0.4069 (4)	0.058
C(233)	0.0914 (12)	0.5950 (7)	0.3788 (5)	0.078
C(234)	0.0613 (6)	0.5911 (6)	0.3251 (5)	0.071
C(235)	0.0533 (11)	0.5154 (9)	0.2995 (3)	0.074
C(236)	0.0755 (13)	0.4435 (6)	0.3276 (6)	0.063
C1(1)	0.8448 (9)	0.3375 (5)	0.1008 (4)	0.105
C1(2)	1.0347 (9)	0.3093 (6)	0.1533 (5)	0.125
H(1)	0.50440	0.19290	0.37270	0.080
H(2)	0.18210	0.18190	0.41310	0.080

[a] $U_{eq} = {}^1/_3\sum_i\sum_j U_{ij}a_i^*a_j^*\mathbf{a}_i\cdot\mathbf{a}_j$.

(7) Ewing, P.; Farrugia, L. J. *Organometallics* **1988**, *7*, 871.

(8) The term radial is here used to define a site with the M–L vector inclined at an angle ~30–40° to the normal to the M_3 face (i.e. trans to a metal–metal bond in a tetrahedron). An axial site is defined as one with the M–L vector approximately perpendicular to the M_3 face, while an equatorial site has the M–L vector coplanar with the M_3 face. Thus, in Figure 1, the atoms P(2) and C(9) are in radial sites, while C(6) is in an axial site, relative to the Os_3 face. The relevant M–L vectors are inclined at angles of 37.4, 29.2, and 4.9°, respectively, to the normal to the Os_3 face. The distinction between axial and radial sites arises because pseudooctahedral geometry is retained at individual Os atoms in these clusters.

(9) Farrugia, L. J. *Adv. Organomet. Chem.* **1990**, *31*, 301.

Table IV. Important Bond Lengths (Å) and Bond Angles (deg) for $Os_3Pt(\mu\text{-}H)_2(CO)_9(Pt\text{-}PCy_3)(Os\text{-}PPh_3)\cdot 0.5CH_2Cl_2$ (3c)

Bond Lengths			
Pt–Os(1)	2.865 (1)	Pt–Os(2)	2.816 (1)
Pt–Os(3)	2.806 (1)	Pt–P(1)	2.356 (4)
Os(1)–Os(2)	2.776 (1)	Os(1)–Os(3)	2.767 (1)
Os(2)–Os(3)	2.761 (1)	Os(1)–P(2)	2.315 (4)
Pt–C(1)	1.86 (1)	Os(1)–C(2)	1.88 (1)
Os(1)–C(3)	1.87 (2)	Os(2)–C(4)	1.85 (1)
Os(2)–C(5)	1.88 (6)	Os(2)–C(6)	1.87 (2)
Os(3)–C(7)	1.91 (2)	Os(3)–C(8)	1.88 (2)
Os(3)–C(9)	1.87 (2)		
Bond Angles			
P(1)–Pt–C(1)	98.1 (5)	Pt–Os(1)–P(2)	170.3 (1)
Os(2)–Os(1)–C(3)	153.3 (5)	P(2)–Os(1)–C(2)	86.4 (4)
P(2)–Os(1)–C(3)	90.7 (5)	H(1)–Os(2)–C(6)	176.1 (4)
C(4)–Os(2)–C(6)	98.4 (6)	C(5)–Os(2)–C(6)	93.0 (6)
Pt–Os(3)–C(9)	159.9 (5)	C(7)–Os(3)–C(9)	95.2 (7)
C(8)–Os(3)–C(9)	89.6 (7)	Os(1)–Os(2)–C(6)	88.9 (4)
Os(3)–Os(2)–C(6)	85.3 (4)	Os(2)–Os(1)–P(2)	114.9 (1)
Os(2)–Os(3)–C(9)	101.3 (5)		

in contrast to that observed in **1**[1a] and **2**,[7] the longest such distance in **3c** is Pt–Os(1) [i.e. the vector trans to the Os–P(2) bond] rather than the hydride-bridged Pt–Os(2) vector. The Os(1)–Os(3) distance of 2.767 (1) Å is unusually short for an Os(μ-H)Os interaction. This is indicative of localized unsaturation, as has been previously discussed.[1b,7] The Os(1)–P(2) and Pt–P(1) distances of 2.315 (4) and 2.356 (4) Å are respectively shorter and longer than the *mean* distances [2.388 (37) and 2.323 (34) Å] recently tabulated by Orpen et al.[10] for these specific M–P separations in a number of complexes.

The Pt–Os(1)–Os(3) face approximates to a triaxial M_3 face[8] (in shorthand $^{aaa}M_3$), since the three M–L vectors Pt–C(1), Os(1)–C(3), and Os(3)–C(7) are inclined at angles of 3.4, 9.7, and 15.4°, respectively, to the normal to this face. The Os_3 face in $Os_3(CO)_{12}$ is of the $^{aaa}M_3$ type,[11] and the diaxial steric interactions between the CO ligands in this structural type are quite significant.[12] There are no known monodentate phosphine derivatives of $M_3(CO)_{12}$ (M = Ru, Os) where axial substitution occurs as a ground-state geometry.[13] Even in the case of the derivative $Os_3(CO)_6[P(OMe)_3]_6$, all six PR_3 ligands are found in equatorial sites, albeit with a D_3 distortion to reduce steric congestion.[14] Indeed several authors[13,15] consider axial phosphines to be unlikely even in the excited states responsible for fluxional behavior. Such considerations therefore imply that phosphine coordination in the axial site occupied by CO(3) in **3c** (Figure 1) is unlikely, even though this site is equatorial relative to the Os_3 plane.

On the other hand, the Os_3 face in **3c** may be described[8] as an axial–radial–radial ($^{arr}M_3$) face. The clusters $Os_3(\mu\text{-}H)_2(CO)_{10}$[16] and $[Re_3(\mu\text{-}H)_4(CO)_{10}]^-$[17] have $^{arr}M_3$ faces, and here the evidence for phosphine substitution is more mixed. Phosphine substitution derivatives of $Os_3(\mu\text{-}H)_2(CO)_{10}$ generally have the phosphine in an equatorial position, but with small phosphines such as PMe_3 there is NMR evidence for isomers with radial-site substitution.[5] The derivative $[Re_3(\mu\text{-}H)_4(CO)_9(PPh_3)]^-$ is highly unusual in having an axial phosphine ligand.[18] The axial–radial steric interactions are evidently less severe in the $^{arr}M_3$ face, although in the case of the Re_3 cluster there may also be kinetic reasons[17] for the isolation of the axial-phosphine derivative. In addition, the presence of M(μ-H)M bridges is thought[19] to relieve some of the steric strain around M_3 faces.

Table V. ^{13}C NMR Parameters for $Os_3Pt(\mu\text{-}H)_2(CO)_9(Pt\text{-}PCy_3)(Os\text{-}PMe_2Ph)$ (3a)

		J,[c] Hz			
reson[a]	chem shift,[b] ppm	Pt–C	P–C	H1–C	H2–C
a	197.3	26		3.2	
b	195.2	36		2.9	
c	189.1		10.5		10.3
d	186.9		7.6		3.6
e	184.3	56		5.6	
f	183.5	36			12.6
g	182.4	29			4.0
h	181.5		7.0		3.5
i	171.9	1534	5.0	36.4	

[a] See Figure 2 and Chart I. [b] 213 K, $CDCl_3$. [c] J error is ±0.5 Hz.

Chart I

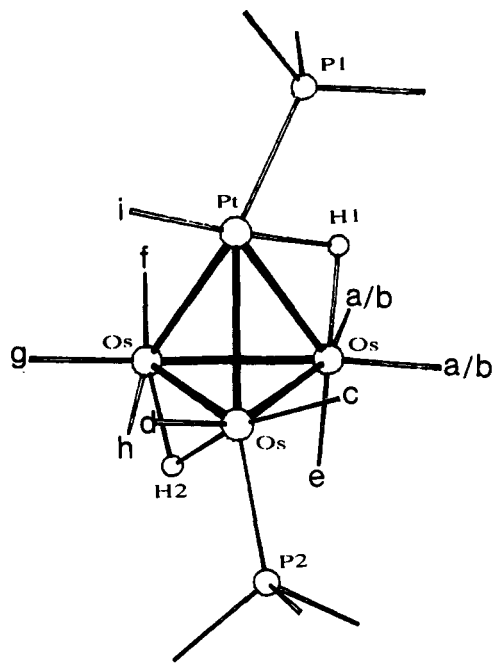

Fluxional Behavior of 3a. The ^1H, ^{31}P, and ^{13}C NMR spectra of **3a** show signals compatible with only one solution species. However, in common with **3b** and particularly **3c** (see below and Figure 6), the low-frequency ^{195}Pt satellite of the ^{31}P resonance from the PCy_3 ligand is noticeably broader at ambient temperature than the high-frequency satellite. This differential broadening of ^{195}Pt satellites has been noted previously[20] and is attributed to a low, undetectable, concentration of a second isomer in exchange with the main species.

The ^{13}C data in the CO region of a ^{13}CO-enriched sample are given in Table V, and the variable-temperature spectra are shown in Figure 2. The assignments to individual

(10) Orpen, A. G.; Brammer, L.; Allen, F. H.; Kennard, O.; Watson, D. G.; Taylor, R. *J. Chem. Soc., Dalton Trans.* **1989**, S1.
(11) Churchill, M. R.; DeBoer, B. G. *Inorg. Chem.* **1977**, *16*, 878.
(12) Lauher, J. W. *J. Am. Chem. Soc.* **1986**, *108*, 1521.
(13) Johnson, B. F. G.; Bott, A. *J. Chem. Soc., Dalton Trans.* **1990**, 2437 and references therein.
(14) Alex, R. F.; Einstein, F. W. B.; Jones, R. H.; Pomeroy, R. K. *Inorg. Chem.* **1987**, *26*, 3175.
(15) Alex, R. F.; Pomeroy, R. K. *Organometallics* **1987**, *6*, 2437.
(16) Broach, R. W.; Williams, J. M. *Inorg. Chem.* **1979**, *18*, 314.
(17) Beringhelli, T.; Ciani, G.; D'Alfonso, G.; Molinari, H.; Sironi, A. *Inorg. Chem.* **1985**, *24*, 2666.
(18) Beringhelli, T.; D'Alfonso, G.; Freni, M.; Ciani, C.; Sironi, A.; Molinari, H. *J. Chem. Soc., Dalton Trans.* **1986**, 2691.
(19) Farrugia, L. J.; Green, M.; Hankey, D. R.; Murray, M.; Orpen, A.; Stone, F. G. A. *J. Chem. Soc., Dalton Trans.* **1985**, 177.
(20) Farrugia, L. J.; Howard, J. A. K.; Mitrprachachon, P.; Stone, F. G. A.; Woodward, P. *J. Chem. Soc., Dalton Trans.* **1981**, 162.

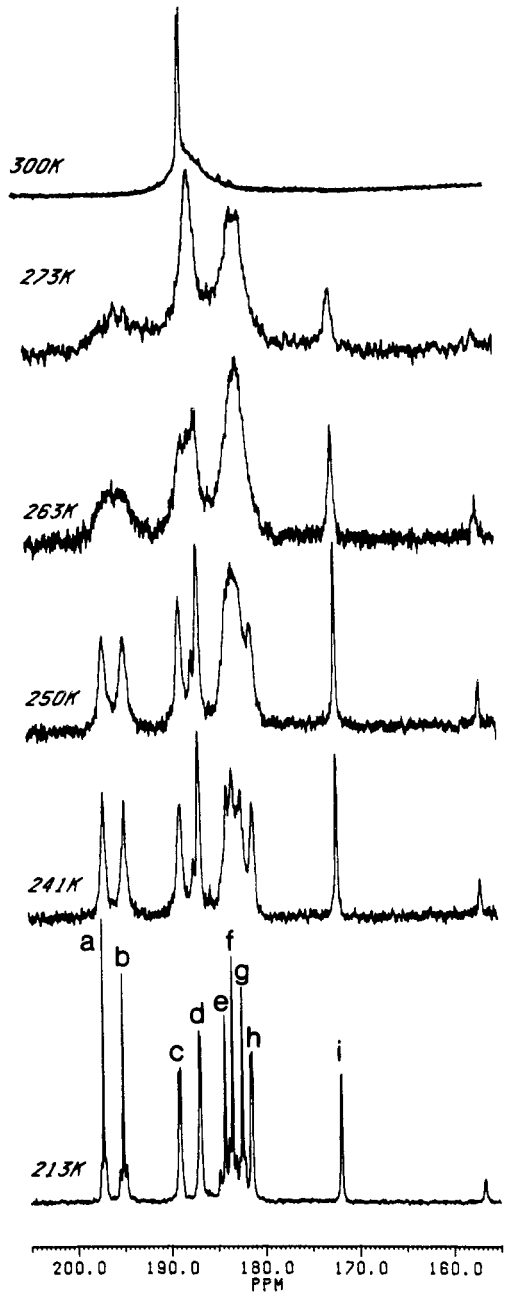

Figure 2. Variable-temperature $^{13}C\{^1H\}$ NMR spectra of **3a** in the carbonyl region.

carbonyls given in Chart I are made on the basis of couplings to the two hydrides. The decoupling difference spectra, shown in Figure 3, clearly demonstrate that the Pt(μ-H)Os hydride couples to only four carbonyls (resonances a, b, e, and i), while the Os(μ-H)Os hydride couples to the remaining five carbonyls. The CO ligands with the largest couplings to each of the hydrides are assigned to those carbonyls that are trans to the hydrides. Due to their ^{31}P couplings and exchange behavior, resonances c and d are assigned to the CO's in the $Os(CO)_2(PMe_2Ph)$ group. The only remaining ambiguities are for the pairs a/b and g/h. The latter are assigned on the basis of ^{31}P and ^{195}Pt couplings as compared with the parent cluster 1.[1b] We are unable to determine the relative assignments of a and b. Since we were also unable to ascertain, from chemical shift or coupling data, whether resonance d arose from an equatorial or radial CO in the $Os(CO)_2(PMe_2Ph)$ group, the site of phosphine substitution was unclear from the NMR data alone. This matter was resolved by the crystal

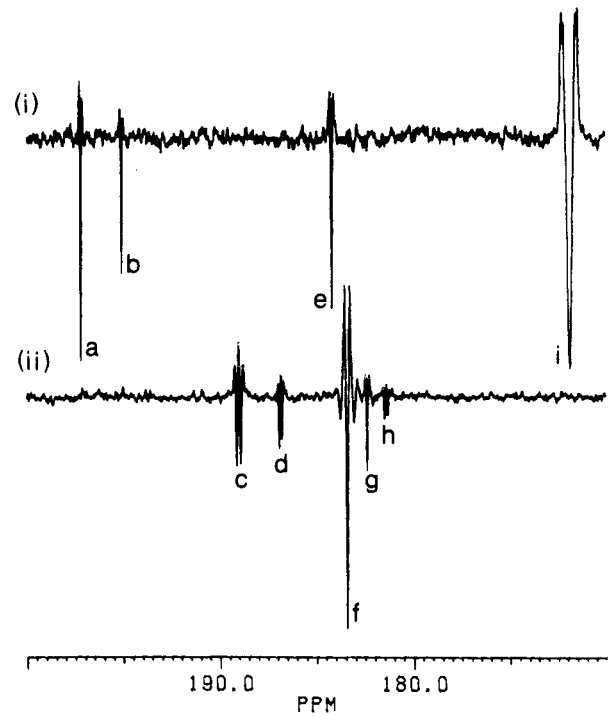

Figure 3. Decoupling difference ^{13}C NMR spectra of **3a** in the carbonyl region, showing difference between the control off-resonance irradiation and (i) irradiation at the Os(μ-H)Pt ^1H frequency and (ii) irradiation at the Os(μ-H)Os ^1H frequency.

structure of **3c** described above.

The variable-temperature spectra in Figure 2 show that resonances c and d collapse at 300 K to an averaged doublet at δ 187.5 [J(P–C) = 8.1 Hz], while other signals collapse to a broad resonance in the same region. Of particular interest is the fact that the Pt-bound CO, resonance i, also broadens at 263 K and collapses with the other signals. In cluster **1**, we have previously observed[1b] that the Pt-bound CO remains uninvolved in the low-energy exchanges and only broadens above 330 K. Thus, in this case, phosphine substitution lowers the barrier to intermetallic CO exchange. This effect has often been observed (see for example ref 15), although there are also examples of the opposite trend, e.g. in $Fe_3(CO)_{12}$.[21] The intermetallic CO exchange in **3a** is localized, since only the unsubstituted $Os(CO)_3$ groups exchange with Pt–CO, while the two CO's in the $Os(CO)_2(PMe_2Ph)$ moiety remain distinct. This intermetallic exchange presumably occurs via a transition state/intermediate that has CO ligands bridging the Pt–Os(2)–Os(3) face. The presence of the phosphine at the Os(1) vertex may prevent the CO's bound to this metal atom being involved in exchange, since phosphines demonstrate a marked reluctance to adopt bridging modes. However, in view of recent results reported by Balch[22] and Puddephatt[23] such bridging modes can no longer be dismissed.

Further information about the CO exchange was provided by a ^{13}C EXSY spectrum shown in Figure 4. The 2D EXSY technique[24] is very powerful in elucidating

(21) Adams, H.; Bailey, N. A.; Bentley, G. W.; Mann, B. E. *J. Chem. Soc., Dalton Trans.* **1989**, 1831.
(22) Balch, A. L.; Davis, B. J.; Olmstead, M. M. *J. Am. Chem. Soc.* **1990**, *112*, 8592.
(23) Bradford, A. M.; Douglas, G.; Manojlović-Muir, Lj.; Muir, K. W.; Puddephatt, R. J. *Organometallics* **1990**, *9*, 409.
(24) (a) Perrin, C. L.; Dwyer, T. J. *Chem. Rev.* **1990**, *90*, 935. (b) Willem, R. *Prog. Nucl. Magn. Reson. Spectrosc.* **1987**, *20*, 1. (c) Orrell, K. G.; Sik, V.; Stephenson, D. *Prog. Nucl. Magn. Reson. Spectrosc.* **1990**, *22*, 141.

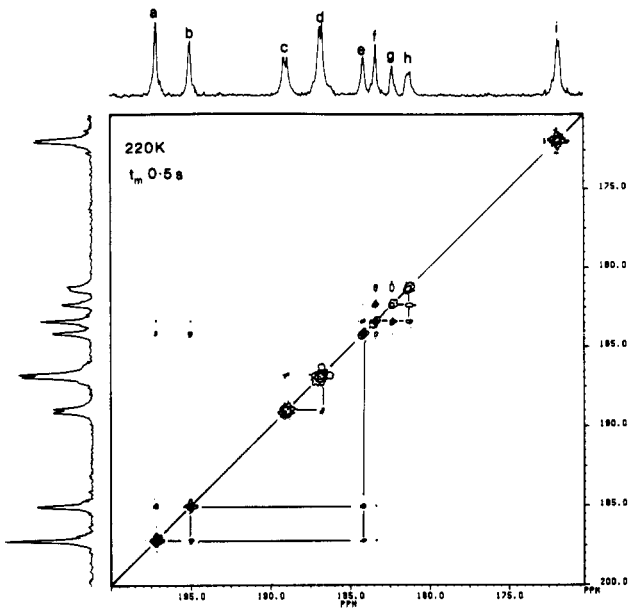

Figure 4. $^{13}C\{^1H\}$ EXSY spectrum of **3a** in the carbonyl region.

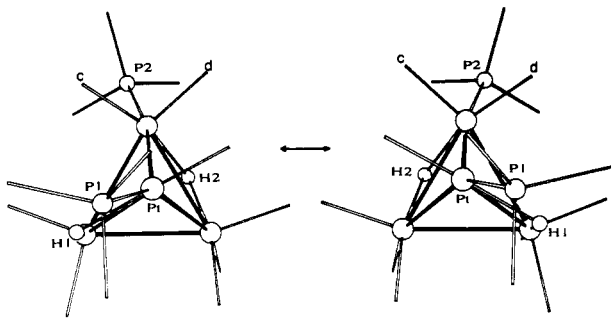

Figure 5. Proposed mechanism for the enantiomerization process in **3a**.

complex exchange pathways and has been used both in a qualitative[1b,25] and quantitative[2,26] fashion to examine carbonyl fluxionality in clusters. In addition to cross peaks confirming the c/d exchange observed in the VT spectra, there are strong cross peaks between resonances a and b and e and also between resonances f and g and h, indicating tripodal rotations in the two $Os(CO)_3$ groups. From the relative intensities of these cross peaks, the e/f/g exchange occurs at a faster rate than the a/b/e exchange, consistent with the behavior observed for **1**.[1b] Weak cross peaks between these two groups of resonances are also observed, indicating a mechanism that renders them chemically equivalent. A 120° "windshield-wiper" motion of the $Pt(H)(CO)(PCy_3)$ group, coupled with a migration of H2 to the adjacent Os–Os edge, as shown in Figure 5, accounts for this observation and also the c/d exchange. The similarities in the activation barriers to exchange of the diastereotopic methyl groups in the PMe_2Ph ligand (ΔG^*_{260} = 53.7 (7) kJ mol^{-1}) and the diastereotopic carbonyls c and d (ΔG^*_{268} = 53.5 (7) kJ mol^{-1}) are fully consistent with a single enantiomerization mechanism. These

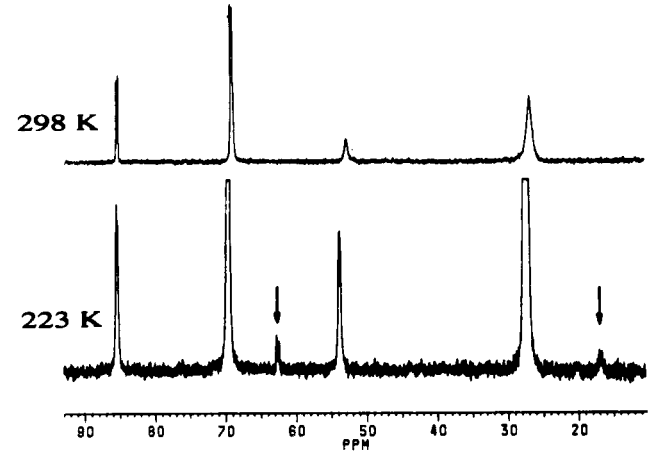

Figure 6. $^{31}P\{^1H\}$ NMR spectra of **3c**, showing differential broadening of resonances. The arrows mark the positions of weak resonances due to the minor isomer.

barriers were estimated from the coalescence temperatures of the methyl and carbonyl signals, respectively, in the ^{13}C spectra.

While we propose a restricted rotation of the $Pt(H)(CO)(PCy_3)$ group, the data do not preclude free rotation of this group about the Os_3 triangular face, which was the case observed for **2**.[2] The presence of the phosphine ligand removes the 3-fold degeneracy of the $Pt(H)L_2$ rotation about the Os_3 triangle, and in the absence of intermetallic phosphine migration, the highest time-averaged symmetry cluster **3a** can achieve is C_s. The very minor isomer of **3a**, which was only detected from the differential broadening of the ^{195}Pt satellites, *may* be a rotameric isomer of the structures shown in Figure 5, but in view of the data for clusters **3d,e** discussed below, we do not think this likely.

The two hydride signals are severely broadened at ambient temperature, and coalescence is observed at 303 K, giving ΔG^*_{303} = 57.1 (6) kJ mol^{-1} for the exchange. Since this value is some 4 kJ mol^{-1} higher than determined for the enantiomerization process, it is unlikely that the latter process involves hydride exchange.

The fluxional behavior of **3b** was not examined in detail, since the ^1H and ^{31}P NMR data (Tables I and II) are very similar to those of **3a** and indicate a single major species is present. The hydrides show site exchange [ΔG^*_{297} = 56.5 (6) kJ mol^{-1}], with a barrier similar to that observed for **3a**.

Fluxional Behavior of 3c. Since the crystal structure of **3c** was used to assign the NMR data for **3a**, it was necessary to confirm that the same structure was adopted in the solid phase and in solution. A solid-state CPMAS ^{31}P spectrum on a crystalline sample of **3c** was obtained, which showed two isotropic shifts at δ 67.2 (J(Pt–P) = 2496 Hz) and δ 33.0. These are close to the solution isotropic values given in Table I and are consistent with structures for **3a–c** in solution identical with that shown in Figure 1.

The differential broadening of the ^{195}Pt satellites observed in the ^{31}P NMR spectra of **3c** at ambient temperatures (Figure 6) is more pronounced than for **3a,b**. The resonance at δ 27.4, due to *Os*-PPh_3, is also substantially broadened, and cooling to 223 K results in sharpening of all signals and the appearance of weak resonances at δ 62.6 and 16.9 [J(P–P) = 30 Hz] due to a minor isomer. The differential broadening is due to the different effective chemical shift separations between exchanging signals. The minor isomer, presumably isomer B (see below), is only present to the extent of ca. 5%. The variable-temperature ^{13}C spectra are very similar to those of **3a** and

(25) (a) Strawczynski, A.; Ros, R.; Roulet, R. *Helv. Chim. Acta* **1988**, *71*, 867. (b) Lindsell, W. E.; Walker, N. M.; Boyd, A. S. F. *J. Chem. Soc., Dalton Trans.* **1988**, 675. (c) Johnson, B. F. G.; Lewis, J.; Pearshall, M.-A.; Scott, L. G. *J. Organomet. Chem.* **1991**, *402*, C27.

(26) (a) Beringhelli, T.; D'Alphonso, G.; Minoja, A. P. *Organometallics* **1991**, *10*, 394. (b) Beringhelli, T.; D'Alphonso, G.; Molinari, H.; Hawkes, G. E.; Sales, K. D. *J. Magn. Reson.* **1988**, *80*, 45. (c) Hawkes, G. E.; Lian, L. Y.; Randall, E. W.; Sales, K. D. *J. Magn. Reson.* **1985**, *65*, 173. (d) Hawkes, G. E.; Lian, L. Y.; Randall, E. W.; Sales, K. D.; Aime, S. *J. Chem. Soc., Dalton Trans.* **1985**, 225.

Figure 7. Variable-temperature ^1H NMR spectra of **3e** in the hydride region.

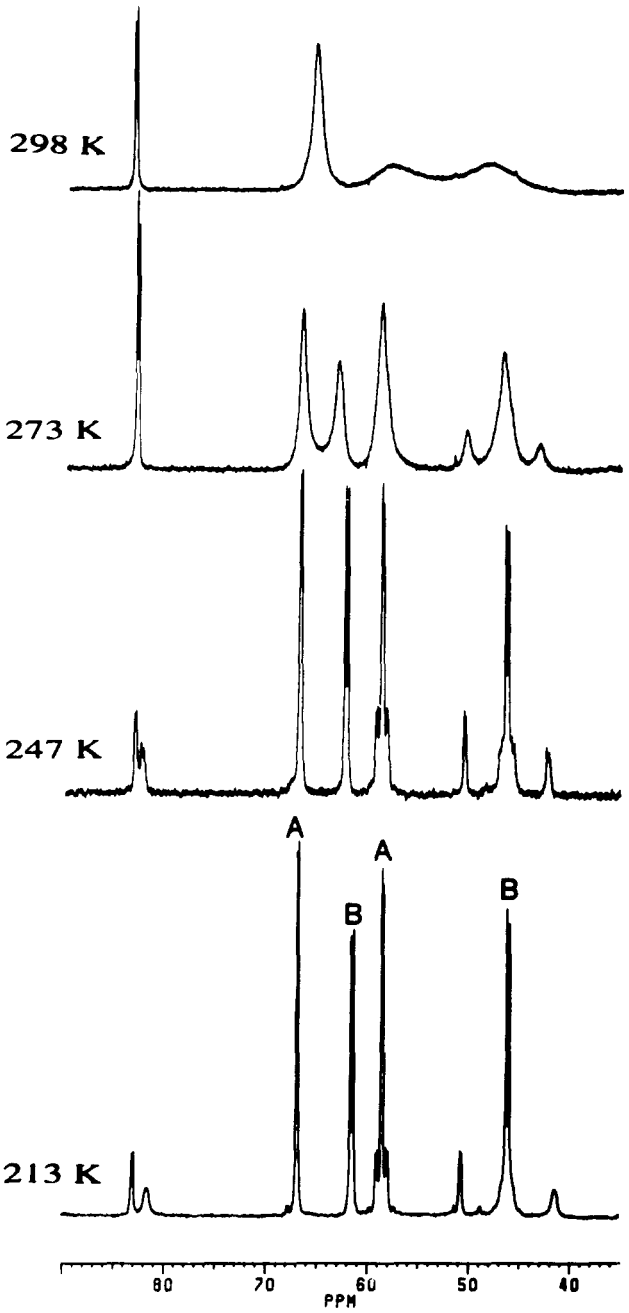

Figure 8. Variable-temperature $^{31}P\{^1H\}$ NMR spectra of **3d**.

indicate that the exchange processes are of comparable energies. They were not examined in detail. The two hydrides undergo site exchange, but due to the overlap with a ^{195}Pt satellite, the coalescence temperature (293 ± 5 K) could not be determined very accurately. This gives $\Delta G^* = 55$ (2) kJ mol^{-1}, which is very similar to that for **3a,b**, indicating that the steric and/or electronic effects of the phosphine on the barriers to interhydride migration are not significant. The exchange barriers are, however, consistently lower than found[1b] for the parent cluster **1**, for which ΔG^*_{295} is 63.1 (5) kJ mol^{-1} for the analogous process.

Fluxional Behavior of 3d,e. The P^iPr_3 and $PCy_2{}^iPr$ derivatives, clusters **3d,e**, exist as a ca. 1:1 isomeric mixture in solution, as shown by their IR spectra in the CO stretching region (Experimental Section) and their NMR data (Tables I and II). The variable-temperature ^1H NMR (hydride region) NMR spectra for **3e** and ^{31}P NMR spectra for **3d** are shown in Figures 7 and 8, respectively. One isomer, A, has very similar parameters associated with the hydrides and ^{31}P signal of the *Pt*-PCy_3 ligand as clusters **3a–c**, and a similar structure is proposed. The second isomer, B, has two inequivalent Os(μ-H)Os hydrides and is much more fluxional. The two hydrides in isomer B undergo a low-energy exchange and appear as a doublet at ca. δ 12.5 in the fast-exchange regime at ~245 K. Above this temperature this resonance broadens due to interisomer exchange, and below this temperature it also broadens due to slowing of the intramolecular hydride exchange. For cluster **3e** (Figure 7) it was possible to estimate this barrier, $\Delta G^*_{206} = 38.8$ kJ mol^{-1}, from the observed coalescence temperature, but we were unable to freeze out the exchange in **3d**. This indicates either that the chemical shifts of the two hydrides are closer in **3d** than **3e** or that the exchange barrier is lower for **3d**. From the averaged ^{31}P coupling of ~7 Hz for the coalesced signal, which is very similar to the cis-^{31}P couplings observed for the Os(μ-H)Os signals in isomer A (Table I), we suggest

Chart II

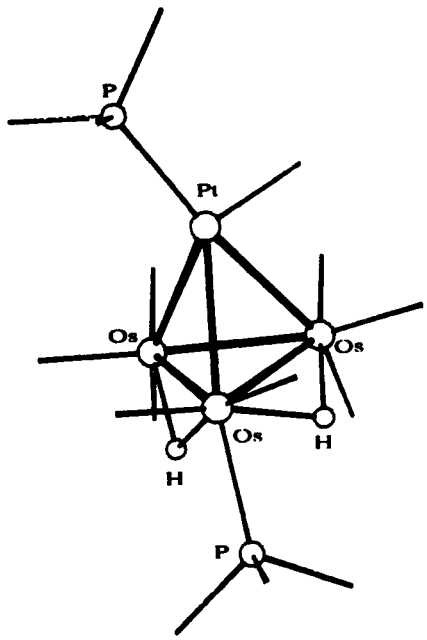

that both the hydrides in isomer B bridge to the Os-$(CO)_2(PR_3)$ vertex.

The orientation of the $Pt(CO)(PCy_3)$ unit relative to the Os_3 triangle in isomer B cannot be determined from the NMR data. Theoretical studies[3] have shown that the favored rotomers have the plane of the PtL_2 unit perpendicular, rather than parallel, to an M–M edge, so that the PCy_3 group could either eclipse a Pt–Os edge (as in **3c**) or lie over a $PtOs_2$ face (as in Chart II). A solid-state ^{31}P CPMAS NMR spectrum of **3d** showed only two isotropic shifts at δ 62.6 (J(Pt–P) = 3280 Hz) and δ 43.4, indicating that isomer B is the structure adopted in the solid state. Unfortunately, no single crystals of either **3d** or **3e** could be obtained. This was particularly frustrating, since **3d** crystallizes in well-formed cubic prisms, but all samples examined proved to be twinned. Only two X-ray structures containing a $Pt(CO)(PR_3)$ moiety capping an Os_3 face have been reported,[19,24] and both have the PR_3 group lying over a $PtOs_2$ face. We hence propose the structure for isomer B shown in Chart II.

The exchange of the hydrides in isomer B can easily be accomplished by a restricted rotation of $Pt(CO)(PCy_3)$ similar to that shown in Figure 5. In this case, however, the process is a degenerate one with no necessity for concomitant hydride migration, and this probably accounts for the much lower barrier. The variable-temperature ^{13}C spectra of **3d** (Figure 9, supplementary material) are fully consistent with the above data. At 247 K there are two sharp signals at δ 186.4 and 176.0 and a very broad signal at ca. δ 185 attributed to isomer B, plus nine slightly broadened signals due to isomer A. On warming, all signals collapse to a broad resonance at 298 K, due to inter- and intraisomer CO scrambling. Due to the complexity of the system, no quantitative analysis was attempted.

The variable-temperature ^1H (Figure 7) and ^{31}P spectra (Figure 10, supplementary material) of **3e** showed additional effects ascribed to a slowing of the rotation of the bulky asymmetric phosphine $PCy_2{}^iPr$ about the Os–P bond. Thus, the resonance due to the Os(μ-H)Os proton of isomer A (δ –7.01 at 248 K) splits into two signals at δ –6.9 and –7.3 (1:2 intensity ratio) on cooling to 180 K. One of the hydride signals of isomer B at δ –11.8 shows a similar decoalescence. The ^{31}P signals of the phosphine ligands (apart from the Pt-PCy_3 ligand in isomer A) also show similar effects on cooling below 243 K. These effects arise because the three rotomers of an asymmetric phosphine bonded to a chiral cluster are inequivalent.

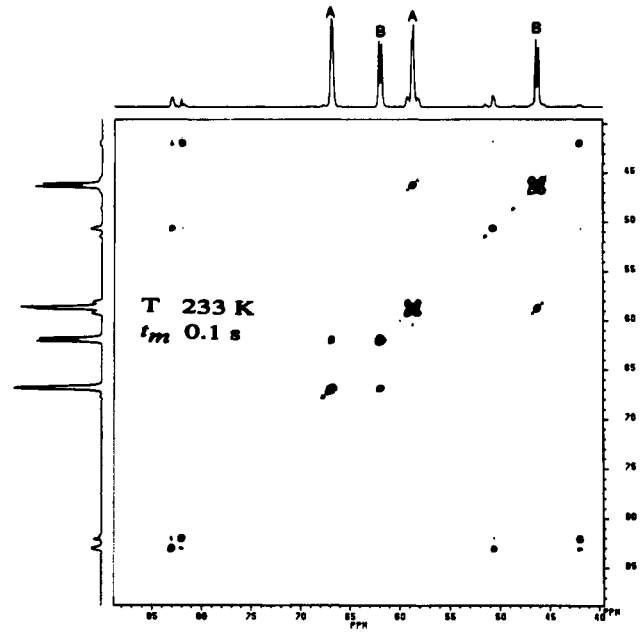

Figure 11. $^{31}P\{^1H\}$ EXSY spectrum of **3d**, showing exchange between isomers A and B.

The exchange between isomers A and B is most easily monitored in the ^{31}P spectrum. These spectra (Figure 8 for **3d**) show several interesting features. Below 247 K, the ^{195}Pt satellites in isomer B are much broader than those for isomer A, indicating a shorter T_1 for the Pt nucleus in isomer B. This may be related to the more facile rotation of the $Pt(CO)(PCy_3)$ unit in this isomer. The high-frequency ^{195}Pt satellites of the Pt-PCy_3 resonances of isomers A and B are at the fast-exchange limit at 298 K due to the proximity of their chemical shifts, and this allows a measurement of the averaged value of J(Pt–P) [2906 Hz for **3d** and 2912 Hz for **3e**]. This in turn allows an estimate of the A:B isomer population of 0.56:0.44 for **3d** and 0.54:0.46 for **3e**.

The ^{31}P EXSY spectrum of **3d** at 233 K (t_m = 0.1 s), shown in Figure 11, displays the expected cross peaks between the Pt-PCy_3 signals in both isomers and between the Os-P^iPr_3 signals in both isomers. The cross peaks that appear between the ^{195}Pt satellites of individual resonances are due to relaxation of the ^{195}Pt nucleus during the mixing time t_m.[27] Analysis of the volume intensities of the diagonal and cross peaks, according to the method of Abel et al.,[28] afforded exchange rate constants between the isomers k_{AB} = 2.37 (18) s^{-1} and k_{BA} = 2.67 (18) s^{-1}. This gave a value of $\Delta G^{\ddagger}_{AB}$ = 54.9 (±1.2) kJ mol^{-1} and a difference in free energies between the two isomers of 0.2 kJ mol^{-1}. The A:B isomer population at 233 K was estimated as 0.53:0.47 from integration of the ^{31}P spectrum. The estimated barrier for interisomer exchange is very similar to those obtained for the hydride migration in clusters **3a–c** and suggests a common mechanistic pathway, which is discussed below.

Conclusions

Our studies on phosphine substitution derivatives of cluster **1** show that, where they can be measured, the

(27) Ruegger, H.; Pregosin, P. S. *Inorg. Chem.* **1987**, *26*, 2912.
(28) Abel, E. W.; Coston, T. P. J.; Orrell, K. G.; Sik, V.; Stephenson, D. *J. Magn. Reson.* **1986**, *70*, 34.

barriers for hydride and carbonyl exchange are lowered by the phosphine ligand. Such effects have been previously noted,[15] and the rationale most commonly put forward is that the phosphine stabilizes bridged structures. As eloquently pointed out by Keister recently,[29] it is notoriously difficult to obtain much information about transition states of fluxional processes from rate data.

Our observation of two almost equally stable structures for **3d** and **3e** in solution poses some interesting questions concerning the hydride migration in **1**. We originally proposed[1b] a mechanism whereby CO and hydride scrambling via μ_3-H intermediates occurred as a single process, but further studies[2] indicated that a common mechanism for hydride and CO scrambling was unlikely. It seems reasonable to suppose that hydride exchange in the closely related clusters **1–3** occurs by a similar mechanism. Our studies reported herein now suggest that this exchange may occur via an intermediate with two Os(μ-H)Os hydrides, i.e. in a stepwise fashion as suggested by Keister.[29] The Os(μ-H)Pt hydride migrates, either across an Os_2Pt face as a μ_3-H intermediate or as a Os–H terminal ligand, to an unoccupied Os–Os edge. In clusters **3a–c** the population of the less stable isomer is very low but may be detected through differential broadening effects in the ^{195}Pt satellites. There was no evidence for a second isomer in the case of **1** or **2**, and the exchange broadening caused by hydride migration could be simulated satisfactorily by assuming a mutual two-site exchange. However, as pointed out by Kaplan,[30] in the case of an A ⇌ B ⇌ C exchange, with no direct A ⇌ C exchange and an undetectable concentration of B, the experimental line shape can often be expressed as a pseudoexchange between A and C. In other words, in these systems, it is not possible to distinguish between an exchange occurring via a symmetric intermediate in very low concentration or a symmetric transition state.

Experimental Section

General experimental techniques were as previously[2] described. NMR spectra were measured on a Bruker AM200 instrument equipped with an FT array processor and process controller. ^{1}H (200.13 MHz) and ^{13}C (50.32 MHz) spectra were referenced to internal solvent signals and are reported relative to $SiMe_4$. ^{31}P (81.02 MHz) spectra are referenced to 85% H_3PO_4. EXSY spectra were recorded either in magnitude mode (^{13}C) or pure absorption mode (^{31}P) by using the Bruker microprogram NOESYPH. ^{13}CO-enriched samples of $Os_3(\mu\text{-H})_2(CO)_9(PR_3)$[5] and $Pt(C_2H_4)_2(PCy_3)$[31] were prepared as previously described.

Preparation of $Os_3Pt(\mu\text{-H})_2(CO)_9(Pt\text{-}PCy_3)(Os\text{-}PMe_2Ph)$ (3a). To a solution of $Os_3(\mu\text{-H})_2(CO)_9(PMe_2Ph)$ (0.3 g, 0.36 mmol) in CH_2Cl_2 (20 mL) was added a solution of $Pt(C_2H_4)_2(PCy_3)$ (0.19 g, 0.36 mmol) in CH_2Cl_2 (10 mL). After being stirred for 1 h, the solution became dark green. The volatiles were removed in vacuo, the residue was redissolved in petroleum ether (bp 40–60 °C), and the solution was chromatographed on a column of Florosil made up in petroleum ether. Elution with dichloromethane/petroleum mixtures afforded a small amount of a light yellow band [shown to be $Os_3(\mu\text{-H})_2\{\mu\text{-C(H)Me}\}(CO)_9(PMe_2Ph)$ from a crystal structure determination on the P^iPr_3 derivative[32]] and a deep green band of cluster **3a**. Removal of solvent gave an oily green residue, in ca. 65% yield, which could not be crystallized. The NMR data were obtained from this oil and showed it to be reasonably pure **3a**.

Clusters **3b–e** were obtained in an analogous fashion, in yields of 30–65%, and were all recrystallized from a petroleum/dichloromethane mixture as black crystals.

Characterizational Data (See Also Tables I, II, and V). **Cluster 3a.** IR (C_6H_{12}): ν(CO) 2059 (m), 2038 (s), 2007 (vs), 1980 (vs), 1974 (vs), 1959 (w), 1940 (m), 1917 cm^{-1} (w). ^{1}H NMR ($CDCl_3$, 298 K): δ 7.6–7.3 (m, 5 H, Ph), 2.5–1.2 (m, 33 H, C_6H_{11}), 1.95 (d, 6 H, Me, J(P–H) = 12 Hz). ^{13}C ($CDCl_3$, 298 K): δ 138.5 (d, 1 C, J(P–C) = 58.1, Ph), 130.4 (d, 1 C, J(P–C) = 2.4 Hz, Ph), 128.7 (d, 2 C, J(P–C) = 17.9 Hz, Ph), 128.7 (d, 2 C, J(P–C) = 1.9 Hz, Ph), 37.0 (d, 3 C, J(P–C) = 21.5, J(Pt–C) = 27.2 Hz, Cy), 29.7 (s, 6 C, J(Pt–C) = 18.2 Hz, Cy), 27.4 (d, 6 C, J(P–C) = 11.2 Hz, Cy), 25.7 (s, 3 C, Cy), 22.5 (d, 2 C, J(P–C) = 40.2 Hz, Me); at 223 K the methyl resonance splits into two signals at δ 21.3 [J(P–C) = 40.2 Hz] and δ 22.3 [J(P–C) = 40.8 Hz].

Cluster 3b. ^{1}H NMR (CD_2Cl_2, 298 K): δ 2.5–1.2 (m, 33 H, Cy), 1.65 (d, 9 H, J(P–H) = 11.2 Hz, Me). Anal. Calcd for $C_{30}H_{44}O_9Os_3P_2Pt$: C, 26.18; H, 3.22. Found: C, 25.96, H, 3.10.

Cluster 3c. IR (C_6H_{12}): ν(CO) 2058 (s), 2037 (s), 2024 (m), 2008 (vs), 1977 (vs), 1968 (w), 1945 (sh), 1938 (m), 1916 (w, sh), 1892 cm^{-1} (w). Anal. Calcd for $C_{45}H_{50}O_9Os_3P_2Pt$: C, 34.59; H, 3.22. Found: C, 33.67; H, 3.02.

Cluster 3d. IR (C_6H_{12}): ν(CO) 2057 (s), 2036 (m), 2018 (vs), 2011 (vs), 1988 (w), 1975 (vs), 1963 (m), 1950 (m), 1945 (w), 1935 (m) 1909 cm^{-1} (w). Anal. Calcd for $C_{36}H_{56}O_9Os_3P_2Pt$: C, 29.61; H, 3.86. Found: C, 29.15; H, 3.56.

Cluster 3e. IR (C_6H_{12}): ν(CO) 2056 (s), 2036 (m), 2016 (vs), 2011 (vs), 1988 (m), 1974 (vs), 1962 (m), 1950 (m), 1934 (m), 1910 cm^{-1} (w). Anal. Calcd for $C_{42}H_{64}O_9Os_3P_2Pt$: C, 32.74; H, 4.19. Found: C, 33.59; H, 4.48.

Crystal Structure Determination. Crystal data are as follows: $C_{45}H_{50}O_9Os_3P_2Pt.^1/_2CH_2Cl_2$, M = 1604.98, monoclinic, space group $P2_1/c$ (No. 14, C_{2h}^5), a = 12.448 (2) Å, b = 16.319 (3) Å, c = 24.936 (5) Å, β = 89.44 (1)°, V = 5065 (2) Å^3, Z = 4, D_c = 2.104 g cm^{-1}, F(000) = 2996, μ(Mo–Kα) = 104.6 cm^{-1}. A black prism of approximate dimensions 0.5 × 0.4 × 0.3 mm was mounted in a general position on a glass fiber and coated with acrylic resin. Data were collected at ambient temperatures, using the $\theta/2\theta$ scan mode, on a CAD4F automated diffractometer with graphite-monochromated X-radiation (λ = 0.71069 Å). Unit cell parameters were determined by refinement of the setting angles (θ = ~12°) of 25 reflections. The intensities of the reflections $5\bar{6}6$, $7\bar{0}2$, and $\bar{2}7\bar{8}$ were monitored every 2 h, and a decay in intensities of ca. 12% over 113 h of data collection was noted, with a linear correction applied. Lp and absorption/extinction corrections (DIFABS;[33] max/min transmission factors 1.32 and 0.83, respectively) were also applied. A total of 8677 measured reflections (θ range 2–24°; h, 0 to 14; k, 0 to 19; l, −29 to +29) yielded 7935 independent data. A total of 5359 reflections having an intensity >3$\sigma(I)$ were considered observed and used for structure solution and refinement. The statistics of the normalized structure factors and systematic absences uniquely indicated the centrosymmetric space group $P2_1/c$. The structure was solved by direct methods (MITHRIL[34]) and subsequent electron density difference syntheses. Refinement was by full-matrix least squares minimizing the function $\sum w(|F_o| - |F_c|)^2$ with the weighting scheme $w = [\sigma^2(F_o)]^{-1}$ used and judged satisfactory. $\sigma(F_o)$ was estimated from counting statistics. All non-H atoms were allowed anisotropic thermal motion, except the atom C(100) in the partially occupied (0.5) dichloromethane molecule of solvation. Hydrogen atoms were refined by using fixed isotropic thermal parameters (U = 0.8 Å^2). The phenyl and cyclohexyl hydrogen atoms were included at calculated positions (C–H = 1.0 Å), as were the metal hydrides (using potential energy minimization methods, HYDEX[35]). The phenyl groups were refined as rigid groups with idealized geometry (C–C = 1.395 Å) and with fixed isotropic thermal parameters (0.08 Å^2) for all H atoms. Due to matrix size limitations, the parameter list was divided into two blocks of 257 and 343 parameters. Refinement converged at R (R_w) = 0.031 (0.042), with mean and maximum Δ/σ values of 0.04 and 0.17, respectively, in the final cycle. A final electron density difference synthesis showed no peaks of chemical significance (maximum $\Delta\rho$ = +1.76, minimum $\Delta\rho$ = −1.09 e Å^{-3} in vicinity of dichloromethane of solvation). The esd of an observation of unit weight (S) was 1.97. Neutral-atom

(29) Nevinger, L. R.; Keister, J. B. *Organometallics* **1990**, *9*, 2312.
(30) Kaplan, J. I. *J. Magn. Reson.* **1988**, *80*, 340.
(31) Spencer, J. L. *Inorg. Synth.* **1979**, *19*, 213.
(32) Farrugia, L. J. Unpublished results.
(33) Walker, N.; Stuart, D. *Acta Crystallogr., Sect. A: Found. Crystallogr.* **1983**, *A39*, 158.
(34) Gilmore, G. J. *J. Appl. Crystallogr.* **1984**, *17*, 42.
(35) Orpen, A. G. *J. Chem. Soc., Dalton Trans.* **1980**, 2509.

scattering factors were taken from ref 36 with corrections applied for anomalous scattering. All calculations were carried out on a MicroVAX 3600 computer using the Glasgow GX suite of programs.[37]

Acknowledgment. Johnson Matthey is thanked for a generous loan of platinum metal salts and the SERC for use of the solid-state NMR facility at Durham, U.K.

Supplementary Material Available: Figures 9 and 10, showing variable-temperature ^{13}C and ^{31}P NMR spectra of cluster **3e**, and tables of anisotropic thermal parameters, calculated hydrogen positional parameters, and complete bond lengths, bond angles, and torsion angles (13 pages); a listing of calculated and observed structure factors (17 pages). Ordering information is given on any current masthead page.

(36) *International Tables for X-Ray Crystallography*; Kynoch: Birmingham, England, 1974; Vol. 4.
(37) Mallinson, P. R.; Muir, K. W. *J. Appl. Chem.* **1985**, *18*, 51.

Synthesis, Structure, and Properties of a Tetranuclear Platinum Cluster Cation

Graeme Douglas,[1a] Ljubica Manojlovic-Muir,*[1a] Kenneth W. Muir,[1a] Michael C. Jennings,[1b] Brian R. Lloyd,[1b] Mehdi Rashidi,[1b,c] Guy Schoettel,[1b] and Richard J. Puddephatt*[1b]

Chemistry Department, University of Glasgow, Glasgow G12 8QQ, Scotland, and Department of Chemistry, University of Western Ontario, London, Ontario N6A 5B7, Canada

Received May 10, 1991

The reaction of $[Pt(O_2CCF_3)_2(dppm)]$ (dppm = $Ph_2PCH_2PPh_2$) with CO/H_2O at 100 °C gives the 58-electron cluster cation $[Pt_4(\mu\text{-}H)(\mu\text{-}CO)_2(\mu\text{-}dppm)_3(dppm\text{-}P)]^+$ (**1**). The structure of $1[PF_6]$ has been determined crystallographically (space group *Pcab* (No. 61), a = 21.120 (6) Å, b = 28.962 (4) Å, c = 31.026 (4) Å, Z = 8) and shown to contain a Pt_4 core in a butterfly geometry. The cluster cation can be considered to be derived from a triangular $Pt_3(\mu\text{-}dppm)_3$ unit, with one edge bridged above by a $Pt(CO)_2(dppm\text{-}P)$ unit and below by a proton. Variable-temperature ^1H, ^{13}C, ^{31}P, and ^{195}Pt NMR spectra show that the cluster cation **1** is fluxional, and the detailed mechanism of this fluxionality has been elucidated by analysis of the coupling constants to ^{195}Pt in the slow- and fast-exchange regions. The cluster core of **1** is robust, but it can be decomposed by H^+ or Ag^+ to give the cluster cation $[Pt_3(\mu_3\text{-}CO)(\mu\text{-}dppm)_3]^{2+}$. Methyl isocyanide displaces the carbonyl ligands of **1** to give $[Pt_4(\mu\text{-}H)(\mu\text{-}CNMe)_2(\mu\text{-}dppm)_3(dppm\text{-}P)]^+$ (**4**). The dppm-*P* ligand of **1** is easily oxidized by O_2 or H_2O_2 to give $[Pt_4(\mu\text{-}H)(\mu\text{-}CO)_2(\mu\text{-}dppm)_3(Ph_2PCH_2P(=O)Ph_2)]^+$ (**5**) and by S_8 or H_2S to give $[Pt_4(\mu\text{-}H)(\mu\text{-}CO)_2(\mu\text{-}dppm)_3(Ph_2PCH_2P(=S)Ph_2)]^+$ (**6**). The reagents Ph_3PAu^+ and $[Pt(O_2CCF_3)_2(dppm)]$ react with **1** to give $[Pt_4(\mu\text{-}AuPPh_3)(\mu\text{-}CO)_2(\mu\text{-}dppm)_3(dppm\text{-}AuPPh_3)][PF_6]_2$ ($7[PF_6]_2$) and $[Pt_4(\mu\text{-}H)(\mu\text{-}CO)_2(\mu\text{-}dppm)_3[dppm\text{-}Pt(O_2CCF_3)(dppm)]][PF_6]_2$ ($8[PF_6]_2$), respectively, by coordination to the dppm-*P* ligand and, in the case of the gold reagent, by isolobal substitution of LAu^+ for H^+. These complexes have been characterized by multinuclear NMR methods.

Introduction

Studies of the chemistry of platinum cluster complexes have been concentrated on the triplatinum clusters, which contain a triangle of platinum atoms.[2-5] However, many higher clusters are known and have been structurally characterized, and there are excellent reviews of this field.[2-4,6] Cluster bonding theories, adapted for platinum's tendency to have a 16-electron rather than 18-electron count, predict that a tetrahedral Pt_4 cluster will be favored for a 56-electron count and that higher electron counts will cause cleavage of metal–metal bonds and opening up of the cluster skeleton.[2,7] Most Pt_4 clusters have a 58-electron count, and in agreement with theory, they adopt a "butterfly" structure, which may be considered to be derived by opening one edge of a tetrahedron.[2-4,7] The clusters $[Pt_4(\mu\text{-}CO)_5(PR_3)_4]$ are good examples of such 58-electron butterfly clusters, and systematic studies have been made of their synthesis, structural and spectroscopic properties, and chemical reactivity.[2-4,8-11]

This paper reports the synthesis of the new 58-electron Pt_4 cluster cation $[Pt_4(\mu\text{-}H)(\mu\text{-}CO)_2(\mu\text{-}dppm)_3(dppm\text{-}P)]^+$ (**1**; dppm = $Ph_2PCH_2PPh_2$) together with a study of its structure, fluxionality, and chemical reactivity. A preliminary account of parts of this work has been published,[12] and the related neutral cluster $[Pt_4(\mu\text{-}CO)_2(\mu\text{-}dppm)_3(Ph_2PCH_2PPh_2{=}O)]$ has also been reported.[13]

Results and Discussion

Synthesis of the Pt_4 Cluster. The reduction of $[Pt(O_2CCF_3)_2(dppm)]$ by carbon monoxide (10 atm) in aqueous methanol at 100 °C gives a useful synthesis of the cluster cation $[Pt_3(\mu_3\text{-}CO)(\mu\text{-}dppm)_3]^{2+}$ (**2**), whose chemistry is very rich.[5] At intermediate stages of reduction, diplatinum(I) complexes such as $[Pt_2H(CO)(\mu\text{-}dppm)_2]^+$

(1) (a) University of Glasgow. (b) University of Western Ontario. (c) Permanent address: Department of Chemistry, Shiraz University, Shiraz, Iran.
(2) Mingos, D. M. P.; Wardle, R. W. M. *Transition Met. Chem.* **1985**, *10*, 441.
(3) Eremko, N. K.; Mednikov, E. G.; Kurasov, S. S. *Russ. Chem. Rev. (Engl. Transl.)* **1985**, *54*, 394.
(4) Clark, H. C.; Jain, V. K. *Coord. Chem. Rev.* **1984**, *55*, 151.
(5) Puddephatt, R. J.; Manojlovic-Muir, Lj.; Muir, K. W. *Polyhedron* **1990**, *9*, 2767.
(6) Chini, P. *J. Organomet. Chem.* **1980**, *200*, 37.
(7) Sappa, E.; Tiripicchio, A.; Carty, A. J.; Toogood, G. E. *Prog. Inorg. Chem.* **1987**, *35*, 437.
(8) Vranka, R. G.; Dahl, L. F.; Chini, P.; Chatt, J. *J. Am. Chem. Soc.* **1969**, *91*, 1574.
(9) Chatt, J.; Chini, P. *J. Chem. Soc. A* **1970**, 1538.
(10) Evans, D. G.; Hallam, M. F.; Mingos, D. M. P.; Wardle, R. W. M. *J. Chem. Soc., Dalton Trans.* **1987**, 1889.
(11) Moor, A.; Pregosin, P. S.; Venanzi, L. M.; Welch, A. J. *Inorg. Chim. Acta* **1984**, *85*, 103.
(12) Douglas, G.; Manojlovic-Muir, Lj.; Muir, K. W.; Jennings, M. C.; Lloyd, B. R.; Rashidi, M.; Puddephatt, R. J. *J. Chem. Soc., Chem. Commun.* **1988**, 149.
(13) Frew, A. A.; Hill, R. H.; Manojlovic-Muir, Lj.; Muir, K. W.; Puddephatt, R. J. *J. Chem. Soc., Chem. Commun.* **1982**, 198.

0276-7333/91/2310-3927$02.50/0